

# Quantum transduction of telecommunications-band single photons from a quantum dot by frequency upconversion

Matthew T. Rakher<sup>1†</sup>, Lijun Ma<sup>2†</sup>, Oliver Slattery<sup>2</sup>, Xiao Tang<sup>2\*</sup> and Kartik Srinivasan<sup>1\*</sup>

**Transducing non-classical states of light from one wavelength to another is required for integrating disparate quantum systems that take advantage of telecommunications-band photons for optical-fibre transmission of quantum information and near-visible, stationary systems for manipulation and storage. In addition, transducing a single-photon source at 1.3  $\mu\text{m}$  to visible wavelengths would be integral to linear optical quantum computation because of near-infrared detection challenges. Recently, transduction at single-photon power levels has been accomplished through frequency upconversion, but it has yet to be demonstrated for a true single-photon source. Here, we transduce triggered single photons from a semiconductor quantum dot at 1.3  $\mu\text{m}$  to 710 nm with 21% (75%) total detection (internal conversion) efficiency. We demonstrate that the upconverted signal maintains the quantum character of the original light, yielding a second-order intensity correlation,  $g^{(2)}(\tau)$ , that shows that the optical field is composed of single photons with  $g^{(2)}(0) = 0.165 < 0.5$ .**

Upconversion is an optical process by which two optical fields combine in a nonlinear medium to generate a third field at a frequency equal to the sum of the two inputs<sup>1</sup>. As well as energy conservation, this process requires momentum conservation, placing a condition on the phase velocities of the three beams. Recently, it has been shown that quasi-phase-matching<sup>2</sup>, a process in which a grating in the nonlinear medium is used to compensate for wave vector mismatch between the sum frequency beam and the two input beams, can enable highly efficient upconversion<sup>3</sup>, with near unity conversion efficiencies achieved in periodically poled LiNbO<sub>3</sub> (PPLN) waveguides. Because upconversion can, in principle, be used to transduce one photon at a given wavelength to a photon at another wavelength, one could imagine using it to couple different quantum systems at different energies<sup>4</sup>. This kind of hybrid quantum-information scheme uses photons for efficient transmission of quantum information over large distances<sup>5</sup>, and robust, stationary quantum systems such as trapped atoms<sup>6</sup> or ions<sup>7</sup>, atomic ensembles<sup>8,9</sup>, or spins in quantum dots<sup>10</sup> for manipulation and storage. Another important application of quantum transduction is the frequency upconversion of telecommunications-band photons to the visible part of the spectrum for detection with commercially available low-noise silicon detectors, for example, as part of a quantum information protocol. The challenges of single photon detection in the near-infrared<sup>11</sup> inhibit the progress of linear optical quantum computation schemes<sup>12,13</sup> because of the stringent requirements on efficient photon detection<sup>14</sup>. Notably, there have been a relatively limited number of upconversion experiments in the quantum domain. In 1992, Huang and Kumar showed that the non-classical intensity correlation between twin beams at 1,064 nm was preserved after one beam was upconverted to 532 nm (ref. 15). In 2001, Kim and colleagues used upconversion to implement a complete Bell state measurement in a quantum teleportation scheme<sup>16</sup>. In 2005, Tanzilli and colleagues demonstrated that the time–energy entanglement between two modes at 1,555 nm and 1,312 nm generated

by spontaneous parametric downconversion was maintained after the 1,312-nm beam was upconverted to 712.4 nm (ref. 17); similar results have also recently been reported for a different set of wavelengths<sup>18</sup>. Although non-classical correlations between the two beams were demonstrated in each case after upconversion, taken individually, each field exhibited classical photon statistics. Recent progress with upconversion detectors has allowed for photo-detection at single-photon power levels<sup>19–22</sup>, although in each case the light detected was a classical source (a highly attenuated laser beam). On the other hand, true (non-classical) single-photon generation has been shown to be achievable through excitation of a single epitaxially grown quantum dot, with experimental demonstrations of stable sources in the 900–1,300 nm region<sup>23–27</sup>, but they have not been used for upconversion. Here, we demonstrate, for the first time, efficient upconversion of single photons generated by a quantum dot at 1.3  $\mu\text{m}$  to 710 nm. In particular, we measure the second-order intensity correlation of the upconverted 710-nm signal, and show that the field is dominantly composed of single photons.

## Optical fibre-based collection of quantum dot emission

In the present experiments, single photons at 1.3  $\mu\text{m}$  were generated by the recombination of excitons in a single epitaxially grown InAs quantum dot embedded in an InGaAs quantum well within a 256-nm-thick GaAs layer. This dot-in-a-well (DWELL) structure enables efficient capture of excitons generated in the quantum well into the quantum dot<sup>28</sup>. Following the work of ref. 29, quantum dots were isolated in a mesa (see Methods), where their emission was collected by a fibre taper waveguide (FTW). A FTW is a single-mode optical fibre, the diameter of which is adiabatically reduced from 125  $\mu\text{m}$  to  $\sim 1 \mu\text{m}$  over 10 mm by simultaneously pulling and heating the fibre with a hydrogen torch to near the melting temperature of glass<sup>30</sup>. Because the diameter is comparable to the wavelength of light, the field exhibits an evanescent tail of a few hundred nanometres outside the physical dimension of the fibre, enabling efficient near-field coupling to

<sup>1</sup>Center for Nanoscale Science and Technology, National Institute of Standards and Technology, Gaithersburg, Maryland 20899, USA, <sup>2</sup>Information Technology Laboratory, National Institute of Standards and Technology, Gaithersburg, Maryland 20899, USA; <sup>†</sup>These authors contributed equally to this work. \*e-mail: xiao.tang@nist.gov; kartik.srinivasan@nist.gov

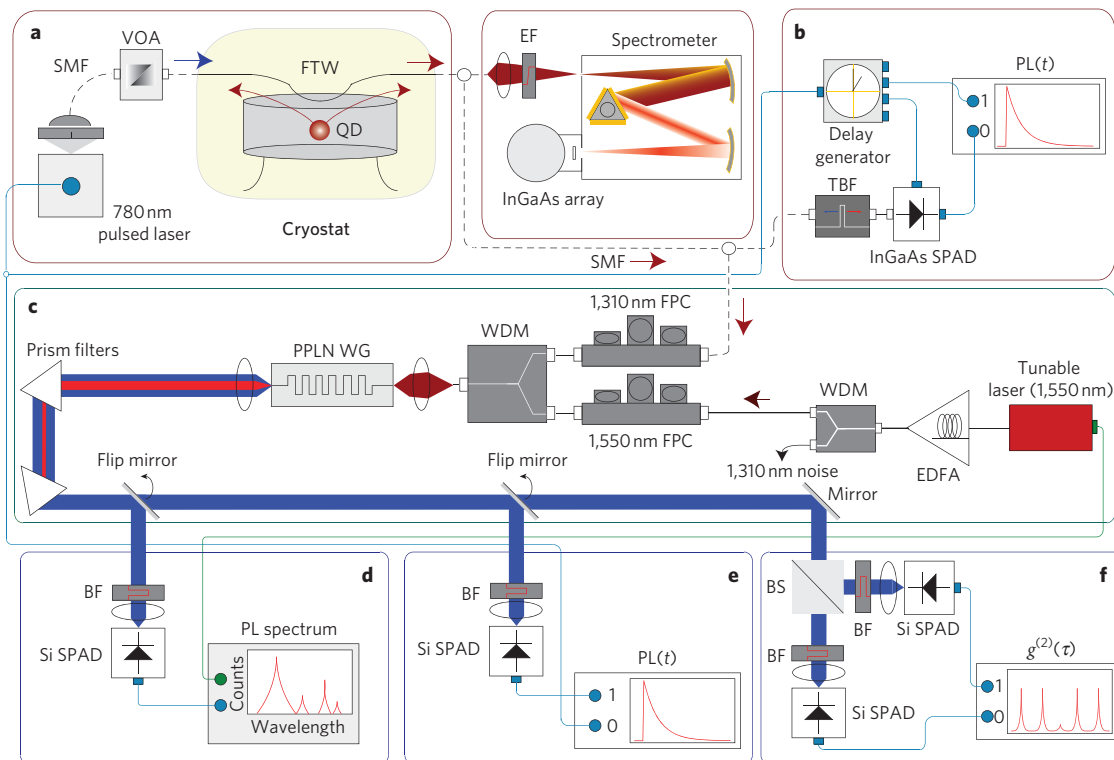


**Figure 1 | Experimental schematic for upconversion of photoluminescence from a quantum dot.** **a**, Schematic of experimental setup for excitation and collection of quantum dot PL by a FTW. **b**, Schematic for time-resolved PL measurement using an InGaAs SPAD. **c**, Upconversion part of the experimental setup. **d**, Schematic for PL spectroscopy after upconversion. **e**, Schematic for time-resolved PL measurement after upconversion. **f**, Schematic of Hanbury-Brown and Twiss interferometer after upconversion. PL, photoluminescence; SPAD, single photon counting avalanche photodiode; FTW, fibre taper waveguide; SMF, single-mode fibre; VOA, variable optical attenuator; FPC, fibre polarization controller; WDM, wavelength division multiplexer; EDFA, erbium-doped fibre amplifier; TBF, tunable bandpass filter; EF, edgepass filter; BF, bandpass filter; BS, non-polarizing beamsplitter; PPLN WG, periodically poled LiNbO<sub>3</sub> waveguide.

nanophotonic devices. As shown in the schematic of Fig. 1a, the quantum dot was optically excited using 50-ps pulses from a 50 MHz laser diode at 780 nm. The laser was directed through a variable optical attenuator and reduced to a power of 10 nW (enough to saturate the single exciton quantum dot transition) before being coupled into the FTW. The FTW was incorporated into a liquid-helium cryostat and positioned in contact with the mesa, which was cooled to  $\sim 8$  K. The evanescent field of the pump laser mode propagating through the FTW excited carriers into the GaAs, where they subsequently optically recombined in the quantum dot, generating photoluminescence (PL). A significant fraction of the photons were emitted back into the FTW and coupled out into the fibre (see Methods). Compared to free-space techniques using a lens or high-numerical-aperture microscope objective, the FTW probe can theoretically collect up to 10 times more photons<sup>31</sup> and provides a natural interface into single-mode fibre for convenient extraction. To measure the quantum dot emission spectrum, we coupled the PL into a grating spectrometer with a cooled InGaAs array with a resolution of  $\sim 0.09$  nm (Fig. 1a). Figure 2a shows such a spectrum with an integration time of 60 s. The sharp lines of a single quantum dot were measured near 1,301.6 nm and 1,302.6 nm, and were identified by polarization to be the positively charged and neutral exciton transitions, respectively, of the same quantum dot. Typical photon fluxes were measured as  $1 \times 10^4$  s<sup>-1</sup>, corresponding to an average power of 1.5 fW. At these low fluxes, InGaAs detectors are difficult to use because of their high dark count rates and lower gain, necessitating long integration times, usually at least an order of magnitude longer than that required for quantum dots with emission near 950 nm where silicon-based detectors can be used.

### Frequency upconversion spectroscopy

For comparison, we also measured the PL spectrum using upconversion, as shown in Fig. 1c,d, following the technique of refs 32, 33 and 34. In this experiment, the PL was directed through a fibre polarization controller (FPC) and combined with a strong optical field near 1,550 nm through a wavelength division multiplexer (WDM). This field was obtained using a tunable diode laser coupled to an erbium-doped fibre amplifier (EDFA), yielding 25–120 mW of continuous power into the PPLN waveguide. The 1,550-nm light was sent through a FPC before being combined with the PL and directed into a 5-cm-long, temperature-controlled PPLN waveguide held at  $61.0 \pm 0.1^\circ\text{C}$ . The strong optical nonlinearity of the PPLN waveguide enables sum-frequency generation under appropriate quasi-phase-matching conditions (bandwidth,  $\sim 0.35$  nm) and creates an optical field near 710 nm where the quantum efficiency of a silicon single photon counting avalanche photodiode (SPAD) is  $\sim 70\%$ . The PPLN waveguide enables upconversion to 710 nm over a broad wavelength range of 1,280–1,340 nm by pump wavelength and temperature adjustment. The light emerging from it is dominantly composed of the upconverted 710-nm signal, the remaining 1,550-nm pump, and frequency-doubled pump photons at 775 nm. To remove the 1,550-nm and 775-nm light, two dispersive prisms and a 20-nm bandpass filter are used before detection at a silicon SPAD. As shown in Fig. 2b, using a laser attenuated to the same power level as the quantum dot emission, we can determine the total detection efficiency (blue) and signal-to-background count ratio (magenta) as a function of 1,550-nm input power (see Methods). The overall detection efficiency maximum is  $21.0 \pm 0.2\%$  for a pump power of 85 mW, and the signal to dark count ratio is maximized for the minimum power of 25 mW. Taking into account optical losses, a lower

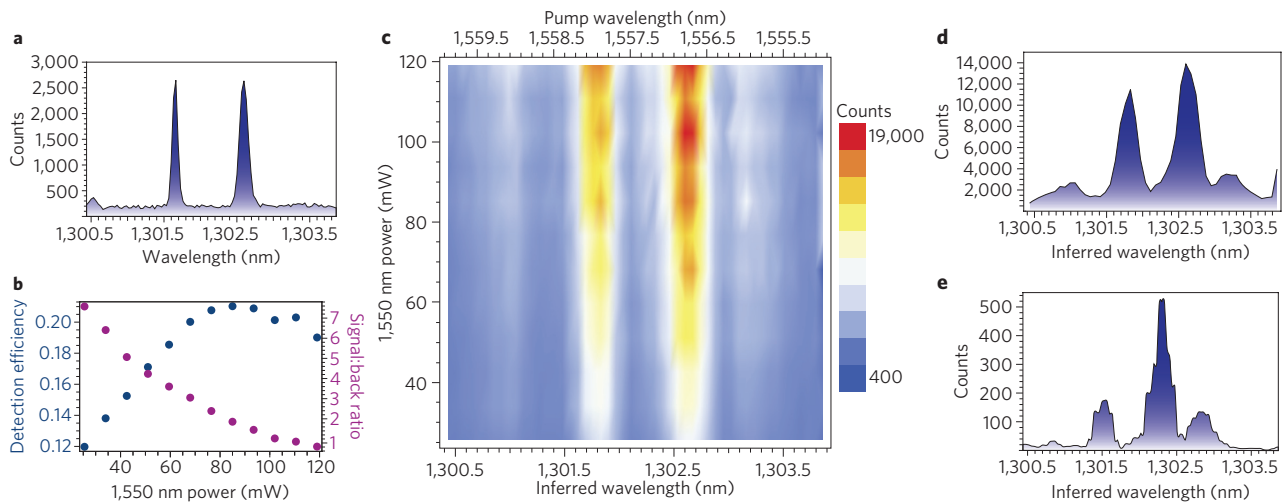


**Figure 2 | Photoluminescence spectrum of a quantum dot measured by upconversion.** **a**, PL spectrum taken with a grating spectrometer with an InGaAs array for an integration time of 60 s. **b**, Total detection efficiency (blue) and signal count to background count ratio (magenta) for upconversion detection as a function of 1,550-nm pump power. **c**, Density plot of the upconverted PL spectrum taken by scanning the 1,550-nm pump laser and integrating 1 s at each point as a function of 1,550-nm pump laser power. **d**, Single upconverted PL spectrum from **c**, with 85 mW of 1,550 nm power. **e**, Upconversion response measured by recording the spectrum of a laser near 1,302.6 nm with 5 MHz linewidth.

bound for the internal conversion efficiency of the PPLN waveguide with 85 mW of 1,550-nm power is estimated to be  $75 \pm 1\%$ . To obtain a spectrum using upconversion, the pump laser was spectrally tuned from 1,555 nm to 1,559.9 nm in 0.1-nm steps while pulses from the silicon SPAD were counted in 1-s bins. In contrast to Fig. 2a, a spectrum was built up through sequential single-channel measurements similar to the action of a scanning monochromator. The resulting spectra as a function of 1,550-nm pump power, pump wavelength and inferred 1,300-nm wavelength are shown in Fig. 2c, and Fig. 2d shows a single spectrum taken with 85 mW of 1,550-nm pump power. Note the presence of both quantum dot emission lines, as in Fig. 2a. The spectrum is limited to a resolution of  $\sim 0.35$  nm and contains side peaks because of the  $\text{sinc}^2$  transfer function response of the PPLN waveguide<sup>2</sup>, as measured directly in Fig. 2e using a narrow linewidth (5 MHz) laser. Although this is a limitation of the use of upconversion for high-resolution spectroscopy, of more importance to subsequent photon counting measurements is the fact that a single-pixel signal-to-noise ratio similar to that of Fig. 2a is obtained for 1/60 the integration time.

### Time-resolved photoluminescence

An important counterpart to the aforementioned steady-state spectroscopy is a time-resolved PL measurement, which can reveal the excited-state lifetime of the quantum dot transition and provide insight into effects such as radiative cascades and non-radiative decay. This measurement can be obtained by incorporating a SPAD and a time-correlated single photon counting (TCSPC) board, as shown schematically in Fig. 1b. The TCSPC repeatedly records the time interval between start events triggered by the pulsed laser and stop events triggered by detection of a photon at the SPAD. First, we used a commercial InGaAs SPAD to measure the lifetime of the neutral exciton (1,302.6 nm) peak after spectral filtering by a tunable 1-nm bandpass filter. Because of the after-pulsing effects associated with InGaAs SPADs<sup>35</sup>, the detector cannot run freely like a silicon SPAD and must run in a gated detection mode as shown in Fig. 1b. Our optimized detection settings were 20% detection probability, 10  $\mu\text{s}$  of dead time and a 20-ns gate width triggered by a delay generator, with the delay chosen to match the detection window to the arrival of pulses of PL. Under this configuration, the trigger rate was 4.3 MHz, and the measured

dark count rate was  $12,500 \text{ s}^{-1}$ . Because of the quantum efficiency oscillations that occur at the start of the gate of our InGaAs detectors, we chose a sufficiently long gate width to avoid these modulations and include the full decay of the PL<sup>26</sup>. The lifetime trace after background subtraction is shown in blue in Fig. 3 for an integration of 700 s. The raw data for the signal (blue) and dark count only (green) measurements are shown in the inset of Fig. 3, where the quantum efficiency oscillations are clearly visible, together with the arrival of the optical pulse at 0 ns. Analysis of the background-subtracted trace leads to a measured lifetime (with 95% confidence interval) of  $1.3 \pm 0.1$  ns, and the resulting fit is shown with the data.

The same lifetime measurement can be performed using a silicon SPAD after upconversion, as shown in Fig. 1e. The PL is combined with 25.5 mW of the pump laser at 1,556.8 nm in the PPLN waveguide for efficient upconversion of the neutral exciton transition at 1,302.6 nm to 710 nm. Because of the 0.35-nm upconversion bandwidth, no additional spectral filtering is required to select the neutral exciton peak. The freely running SPAD (dead time, 50 ns; intrinsic dark count rate,  $100 \text{ s}^{-1}$ ) provides the stop signal for TCSPC, and we integrate for 600 s. To remove background counts, a measurement without the 780-nm excitation is also taken for subsequent subtraction. The resulting measurement is shown in maroon in Fig. 3, and has been temporally offset for comparison with the InGaAs measurement. A fit to the data (red line) yields a lifetime (with 95% confidence interval) of  $1.38 \pm 0.03$  ns. Figure 3 clearly shows the silicon measurement has a dynamic range that is  $\sim 25$  times better than that of the InGaAs SPAD, and demonstrates the usefulness of upconversion for substantially more sensitive detection.

### Second-order intensity correlation

To prove that the upconverted 710-nm signal was composed of single photons and inherently non-classical, we measured the second-order intensity correlation  $g^{(2)}(\tau) = \langle I(t)I(t+\tau) \rangle / \langle I(t) \rangle^2$  using a Hanbury–Brown and Twiss interferometer as depicted in Fig. 1f. After upconversion in the PPLN waveguide pumped by 85 mW of 1,556.8-nm power and spectral dispersion by the prisms, the 710-nm signal was divided by a 50:50 non-polarizing beamsplitter and then directed into two silicon SPADs, where detection events were used as the start and stop signals for the TCSPC. The histogram of such start–stop events as a function of the time

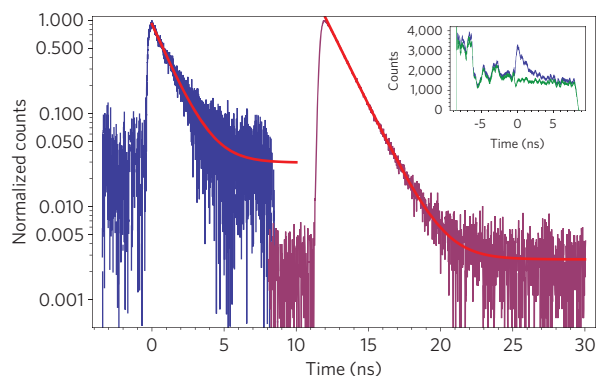


**Figure 3 | Time-resolved photoluminescence of a single quantum dot.** PL lifetime measured by the InGaAs SPAD (blue) and the silicon SPAD (maroon) after upconversion. Inset: raw histograms of the signal (blue) and dark count only (green) traces taken with the InGaAs SPAD.

interval is directly related to  $g^{(2)}(\tau)$ , and is shown in Fig. 4a. The data show that the areas between PL pulses every 20 ns have a non-zero number of events. Clearly, this time-independent background arises from start–stop events triggered by detection of photons not from the PL of the quantum dot, which decays on a fast timescale ( $\tau_{\text{PL}} = 1.38$  ns, as in Fig. 3) every 20 ns. The origin of these events is the start and/or stop detection of upconverted anti-Stokes Raman (ASR) photons near 1,302.6 nm from the pump laser at 1,556.8 nm, which are transmitted by the 20-nm bandpass filter and comprise approximately one-third of the total counts (see Fig. 2b). Nonetheless, the peak at  $\tau=0$  is reduced compared to the other peaks by a factor of  $(0.37 \pm 0.02) < 0.5$ , indicating the

single photon nature of the light. However, because the ASR photon events are temporally distinguishable from true PL events, this background can be subtracted (see Methods) to obtain the true  $g^{(2)}(\tau)$  for the PL signal. In principle, the background can be easily reduced by using smaller-bandwidth filters; for example, a 1-nm filter would reduce it by a factor of  $\sim 20$ . Another feature of Fig. 4a is that the peaks nearest  $\tau=0$  at  $\tau = \{\pm 20$  ns,  $\pm 40$  ns} do not recover completely, even though the quantum dot lifetime is only 1.38 ns. This submicrosecond correlation effect has been measured previously for quantum dots<sup>36</sup> and is thought to be caused by the preferential capture of single carriers into the quantum dots rather than electron–hole pairs. The strength of this effect is known to depend strongly on excitation wavelength and power, and is not the focus of this work. After background subtraction and normalization by peaks far from  $\tau=0$ ,  $g^{(2)}(\tau)$  can be extracted as shown in Fig. 4b. The reduction at  $\tau=0$  is a clear indication of photon antibunching and the non-classical nature of the optical field. The value  $g^{(2)}(0)$  can be obtained by comparing counts in the  $\tau=0$  peak to the average of those in the  $\tau \neq 0$  peaks, and we obtain a value of  $g^{(2)}(0) = 0.165 \pm 0.010$ . Because  $g^{(2)}(0) = 0.165 < 0.5$ , the optical field must be dominantly composed of single photons. The measured non-zero value of  $g^{(2)}(0) = 0.165$  is due to uncorrelated emission at 1.3  $\mu\text{m}$  collected by the FTW and subsequently upconverted, which may be reduced by exciting closer to the quantum dot transition. In addition, the 1,550-nm pump power might also be expected to influence the  $g^{(2)}(0)$  value and the signal-to-noise given tradeoffs between increased detection efficiency and higher levels of background photons, as shown in Fig. 2b. To that end, we performed the  $g^{(2)}(\tau)$  measurement at three values of the 1,550-nm pump power, and the results are displayed in Fig. 4c. The best result (Fig. 4b) was obtained for 85 mW of power, which corresponds to the optimum overall detection efficiency (21.0%) of our set-up.

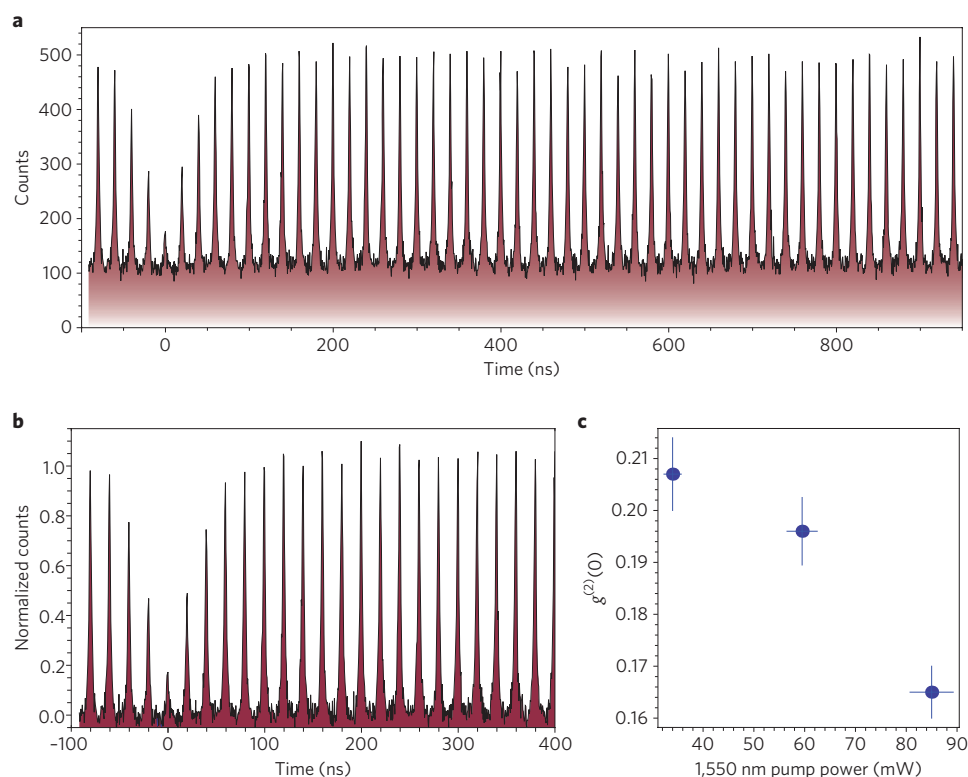


**Figure 4 | Upconversion of single photons.** **a**, Raw histogram of the second-order intensity correlation measurement after 3,600 s. **b**, Normalized second-order intensity correlation  $g^{(2)}(\tau)$  after ASR photon event subtraction. **c**,  $g^{(2)}(0)$  values with errors (see Methods) for different powers of the 1,550-nm pump laser.

## Conclusions

In conclusion, we have used frequency upconversion in a PPLN waveguide to efficiently measure single-photon PL from a quantum dot emitting near 1.3  $\mu\text{m}$  with silicon SPADs. In doing so, we have demonstrated that upconversion can be used for high signal-to-noise spectrometry and time-correlated photon counting for lifetime measurements. Although other groups have shown that superconducting single-photon detectors can be used instead of InGaAs SPADs for such measurements in the near-infrared<sup>37</sup>, those detectors are not yet widely available and require cryogenic cooling, whereas efficient upconversion can be performed with off-the-shelf components. Additionally, we have shown that the quantum-mechanical nature of the single-photon stream emitted by the quantum dot at 1.3  $\mu\text{m}$  is successfully transduced over to a 710-nm optical field, and in particular we measure  $g^{(2)}(0) = 0.165$  for this field. As well as the clear advantage offered in increased measurement sensitivity, efficient quantum transduction by frequency upconversion has several consequences for quantum information schemes involving stationary quantum systems and photons. Because of the large upconversion wavelength range afforded by the quasi-phase-matching of the PPLN waveguide, quantum dots with different emission wavelengths as large as several nanometres (to be expected due to quantum dot growth inhomogeneity) can all be upconverted to the same wavelength. A clear implication of this is that remote operations in the telecommunications band, such as the generation of entanglement<sup>38</sup> between spatially separated electron spins in quantum dots, is possible without the fine spectral-tuning typically required in such schemes. Furthermore, one can envision photon-mediated interactions between electron or hole spins in quantum dots in the near-infrared with alkali atoms or ions in the near-visible. For example, a hole confined in a quantum dot with an optical transition at 1.3  $\mu\text{m}$  could be coupled to a rubidium atom or ensemble<sup>39</sup> at 780 nm by upconversion with a thulium-doped fibre laser at 1.95  $\mu\text{m}$ . Finally, because the upconversion process depends critically on the strong pump field, fast temporal sampling of the input field is possible by using ultrafast pump pulses<sup>40,41</sup>. At present, many time-dependent measurements of quantum dot PL are at best limited to a resolution of  $\sim 40$  ps by the silicon SPAD timing jitter. Given that pulse widths as short as 4.3 fs have been created using mode-locked fibre lasers<sup>42</sup>, quantum dot dynamics on ultrafast timescales could be revealed by upconversion.

## Methods

**Mesa fabrication.** The quantum dot-containing GaAs layer was isolated 1.5  $\mu\text{m}$  above the rest of the sample surface in a 2- $\mu\text{m}$ -diameter mesa. The physical isolation enables efficient probing of a limited number of quantum dots by the FTW. These mesas were created in several steps: (i) electron-beam lithography, (ii)  $\text{SF}_6/\text{C}_4\text{F}_8$  inductively coupled plasma reactive ion etching (ICP-RIE) of a deposited  $\text{Si}_x\text{N}_y$  mask layer, (iii)  $\text{Ar-Cl}_2$  ICP-RIE etching of the GaAs layer and removal of the remaining  $\text{Si}_x\text{N}_y$  layer, and (iv) 20:1  $\text{H}_2\text{O}:\text{HF}$  wet etching of the underlying  $\text{Al}_{0.7}\text{Ga}_{0.3}\text{As}$  layer to form the supporting pedestal.

**FTW PL collection efficiency.** The FTW PL collection efficiency was determined from the measured silicon SPAD count rates corrected for the total detection efficiency (21%) and then normalized to the 50 MHz excitation repetition rate. The normalization was the maximum rate of photon emission by the quantum dot, assuming it was excited a single time for each pump pulse. This assumption is valid because the pulse width (50 ps) is much shorter than the radiative lifetime (1.38 ns) and the average power is such that the transition is saturated. For this quantum dot, which resides in a non-undercut portion of the mesa, we obtained an efficiency near 0.1%. This efficiency is consistent with previous experimental work<sup>29</sup>, and matches theoretical predictions<sup>31</sup> for a non-undercut dielectric substrate.

**Detection and conversion efficiencies.** The overall detection efficiency of 21% was determined with a laser attenuated to a measured power equivalent to the quantum dot (1.5 fW) and set at the wavelength of the neutral exciton transition. The measured silicon SPAD count rates after background subtraction were compared to the known input power level. The internal conversion efficiency of 75% was calculated by correcting the overall efficiency for the measured optical losses ( $\eta_{\text{WDM}} = 0.95$ , in-coupling and transmission through the PPLN waveguide

$\eta_{\text{PPLN}} = 0.61$ , beamsplitter and mirror loss  $\eta_{\text{BS}} = 0.81$ , and  $\eta_{\text{BF}} = 0.85$ ) and silicon SPAD quantum efficiency at 710 nm ( $\eta_{\text{SPAD}} = 0.70$ ). The errors in both efficiencies dominantly result from shot noise in the photon counts. Including the PL collection efficiency, the end-to-end efficiency of the system was  $\sim 0.02\%$ .

**$g^{(2)}(\tau)$  background subtraction.** As described in the main text, background counts were due to ASR photon events and were time-independent. The subtracted level was determined by taking the average number of counts measured for time delays greater than 8.2 ns from the nearest PL pulse. Because the lifetime was measured to be 1.38 ns, the probability of a PL event contributing at these time delays was negligible ( $\sim 0.3\%$ ). The background counts observed in the measurement were consistent with what was expected from the ratio of signal-to-background counts measured in Fig. 2b for 85 mW of pump power. Errors in the extracted  $g^{(2)}(0)$  values were determined by the propagation of errors due to shot noise in the  $\tau = 0$  peak area, the standard deviation of the peak areas far from  $\tau = 0$ , and the shot noise in the subtracted background level.

Received 10 May 2010; accepted 19 August 2010;

published online 3 October 2010

## References

- Boyd, G. D. & Kleinman, D. A. Parametric interaction of focused Gaussian light beams. *J. Appl. Phys.* **39**, 3597–3639 (1968).
- Fejer, M. M., Magel, G. A., Jundt, D. H. & Byer, R. L. Quasi-phase-matched second harmonic generation – tuning and tolerances. *IEEE J. Quantum Electron.* **28**, 2631–2654 (1992).
- Chanvillard, L. *et al.* Soft proton exchange on periodically poled LiNbO<sub>3</sub>: a simple waveguide fabrication process for highly efficient nonlinear interactions. *Appl. Phys. Lett.* **76**, 1089–1091 (2000).
- Wallquist, M., Hammerer, K., Rabl, P., Lukin, M. & Zoller, P. Hybrid quantum devices and quantum engineering. *Physica Scripta* **2009**, 014001 (2009).
- Marcikic, I., de Riedmatten, H., Tittel, W., Zbinden, H. & Gisin, N. Long-distance teleportation of qubits at telecommunication wavelengths. *Nature* **421**, 509–513 (2003).
- Boozer, A. D., Boca, A., Miller, R., Northup, T. E. & Kimble, H. J. Reversible state transfer between light and a single trapped atom. *Phys. Rev. Lett.* **98**, 193601 (2007).
- Olmschenk, S. *et al.* Quantum teleportation between distant matter qubits. *Science* **323**, 486–489 (2009).
- Duan, L., Lukin, M. D., Cirac, J. I. & Zoller, P. Long-distance quantum communication with atomic ensembles and linear optics. *Nature* **414**, 413–418 (2001).
- Chaneliere, T. *et al.* Storage and retrieval of single photons transmitted between remote quantum memories. *Nature* **438**, 833–836 (2005).
- Gerardot, B. D. *et al.* Optical pumping of a single hole spin in a quantum dot. *Nature* **451**, 441–444 (2008).
- Hadfield, R. H. Single-photon detectors for optical quantum information applications. *Nature Photon.* **3**, 696–705 (2009).
- Knill, E., Laflamme, R. & Milburn, G. J. A scheme for efficient quantum computation with linear optics. *Nature* **409**, 46–52 (2001).
- Kok, P. *et al.* Linear optical quantum computing with photonic qubits. *Rev. Mod. Phys.* **79**, 135–174 (2007).
- Varnava, M., Browne, D. E. & Rudolph, T. How good must single photon sources and detectors be for efficient linear optical quantum computation? *Phys. Rev. Lett.* **100**, 060502 (2008).
- Huang, J. M. & Kumar, P. Observation of quantum frequency conversion. *Phys. Rev. Lett.* **68**, 2153–2156 (1992).
- Kim, Y.-H., Kulik, S. P. & Shih, Y. Quantum teleportation of a polarization state with a complete Bell state measurement. *Phys. Rev. Lett.* **86**, 1370–1373 (2001).
- Tanzilli, S. *et al.* A photonic quantum information interface. *Nature* **437**, 116–120 (2005).
- Ma, L., Slattery, O., Chang, T. & Tang, X. Non-degenerated sequential time-bin entanglement generation using periodically poled KTP waveguide. *Opt. Express* **17**, 15799–15807 (2009).
- Vandevender, A. & Kwiat, P. High efficiency single photon detection via frequency up-conversion. *J. Mod. Opt.* **51**, 1433–1445 (2004).
- Langrock, C. *et al.* Highly efficient single-photon detection at communication wavelengths by use of upconversion in reverse-proton-exchanged periodically poled LiNbO<sub>3</sub> waveguides. *Opt. Lett.* **30**, 1725–1727 (2005).
- Albota, M. & Wong, F. Efficient single-photon counting at 1.55  $\mu\text{m}$  by means of frequency upconversion. *Opt. Lett.* **29**, 1449–1451 (2004).
- Xu, H., Ma, L., Mink, A., Hershman, B. & Tang, X. 1310-nm quantum key distribution system with up-conversion pump wavelength at 1550 nm. *Opt. Express* **15**, 7247–7260 (2007).
- Michler, P. *et al.* A quantum dot single-photon turnstile device. *Science* **290**, 2282–2285 (2000).
- Pelton, M. *et al.* Efficient source of single photons: a single quantum dot in a micropost microcavity. *Phys. Rev. Lett.* **89**, 233602 (2002).

25. Strauf, S. *et al.* High-frequency single-photon source with polarization control. *Nature Photon.* **1**, 704–708 (2007).
26. Zinoni, C. *et al.* Time-resolved and antibunching experiments on single quantum dots at 1300 nm. *Appl. Phys. Lett.* **88**, 131102 (2006).
27. Shields, A. J. Semiconductor quantum light sources. *Nature Photon.* **1**, 215–223 (2007).
28. Stintz, A., Liu, G. T., Li, H., Lester, L. F. & Malloy, K. J. Low-threshold current density 1.3- $\mu\text{m}$  InAs quantum-dot lasers with the dots-in-a-well (DWELL) structure. *IEEE Photon. Tech. Lett.* **12**, 591–593 (2000).
29. Srinivasan, K., Painter, O., Stintz, A. & Krishna, S. Single quantum dot spectroscopy using a fiber taper waveguide near-field optic. *Appl. Phys. Lett.* **91**, 091102 (2007).
30. Knight, J. C., Cheung, G., Jacques, F. & Birks, T. A. Phase-matched excitation of whispering-gallery-mode resonances by a fiber taper. *Opt. Lett.* **22**, 1129–1131 (1997).
31. Davanço, M. & Srinivasan, K. Efficient spectroscopy of single embedded emitters using optical fiber taper waveguides. *Opt. Express* **17**, 10542–10563 (2009).
32. Ma, L., Slattery, O. & Tang, X. Experimental study of high sensitivity infrared spectrometer with waveguide-based up-conversion detector. *Opt. Express* **17**, 14395–14404 (2009).
33. Thew, R. T., Zbinden, H. & Gisin, N. Tunable upconversion photon detector. *Appl. Phys. Lett.* **93**, 071104 (2008).
34. Zhang, Q., Langrock, C., Fejer, M. M. & Yamamoto, Y. Waveguide-based single-pixel up-conversion infrared spectrometer. *Opt. Express* **16**, 19557–19561 (2008).
35. Ribordy, G. *et al.* Photon counting at telecom wavelengths with commercial InGaAs/InP avalanche photodiodes: current performance. *J. Mod. Opt.* **51**, 1381–1398 (2004).
36. Santori, C. *et al.* Submicrosecond correlations in photoluminescence from InAs quantum dots. *Phys. Rev. B* **69**, 205324 (2004).
37. Zinoni, C. *et al.* Single-photon experiments at telecommunication wavelengths using nanowire superconducting detectors. *Appl. Phys. Lett.* **91**, 031106 (2007).
38. Simon, C. *et al.* Quantum communication with quantum dot spins. *Phys. Rev. B* **75**, 081302 (2007).
39. Eisaman, M. D. *et al.* Electromagnetically induced transparency with tunable single-photon pulses. *Nature* **438**, 837–841 (2005).
40. Kuzucu, O., Wong, F. N. C., Kurimura, S. & Tovstonog, S. Time-resolved single-photon detection by femtosecond upconversion. *Opt. Lett.* **33**, 2257–2259 (2008).
41. Shah, J. Ultrafast luminescence spectroscopy using sum frequency generation. *IEEE J. Quantum Electron* **24**, 276–288 (1988).
42. Krauss, G. *et al.* Synthesis of a single cycle of light with compact erbium-doped fibre technology. *Nature Photon.* **4**, 33–36 (2009).

### Acknowledgements

The authors thank A. Stintz and S. Krishna of the University of New Mexico and O. Painter of the California Institute of Technology for assistance with sample preparation, and M. Davanço of NIST for development of the fibre taper fabrication setup.

### Author contributions

M.T.R. and K.S. built the low-temperature measurement setup. L.M., O.S. and X.T. built the upconversion detectors. K.S. fabricated the devices and M.T.R., L.M. and K.S. performed the measurements. M.T.R. and K.S. wrote the manuscript. All authors contributed to the design of the experiments, and K.S. and X.T. supervised the project.

### Additional information

The authors declare no competing financial interests. Reprints and permission information is available online at <http://npg.nature.com/reprintsandpermissions/>. Correspondence and requests for materials should be addressed to K.S.